Journal of Oceanology and Limnology
Vol. 39 No. 6, P. 2116-2126, 2021
https://doi.org/10.1007/s00343-021-1071-4

Determination of the heating efficiency of magnetotactic bacteria in alternating magnetic field*

Tongwei ZHANG[1, 2, 3, 4], Huangtao XU[1, 2, 3, 4], Jia LIU[1, 2, 4], Yongxin PAN[1, 2, 3, 4], Changqian CAO[1, 2, 4, **]

[1] *Key Laboratory of Earth and Planetary Physics*, *Institute of Geology and Geophysics*, *Innovation Academy for Earth Science*, *Chinese Academy of Sciences*, *Beijing 100029*, *China*

[2] *Innovation Academy for Earth Science*, *Chinese Academy of Sciences*, *Beijing 100029*, *China*

[3] *College of Earth and Planetary Sciences*, *University of Chinese Academy of Sciences*, *Beijing 100049*, *China*

[4] *France-China Joint Laboratory for Evolution and Development of Magnetotactic Multicellular Organisms*, *Chinese Academy of Sciences*, *Beijing 100029*, *China*

Received Mar. 1, 2021; accepted in principle Mar. 23, 2021; accepted for publication Apr. 30, 2021
© Chinese Society for Oceanology and Limnology, Science Press and Springer-Verlag GmbH Germany, part of Springer Nature 2021

Abstract Magnetotactic bacteria (MTB) intact cells have been applied in magnetic hyperthermia therapy of tumor, showing great efficiency in heating for tumor cell inhibition. However, the detailed magnetic hyperthermia properties and optimum heat production conditions of MTB cells are still poorly understood due to lack of standard measuring equipment. The specific absorption rate (SAR) of MTB cells is often measured by home-made equipment at a limited frequency and magnetic field amplitude. In this study, we have used a commercial standard system to implement a comprehensive study of the hyperthermic response of *Magnetospirillum gryphiswaldense* MSR-1 strain under 7 frequencies of 144–764 kHz, and 8 field amplitudes between 10 and 45 kA/m. The measurement results prove that the SAR of MTB cells increases with magnetic field frequency and amplitude within a certain range. In combination with the magnetic measurements, it is determined that the magnetic hyperthermia mechanism of MTB mainly follows the principle of hysteresis loss, and the heat efficiency of MTB cells in alternating magnetic field are mainly affected by three parameters of hysteresis loop, saturation magnetisation, saturation remanent magnetisation, and coercivity. Thus when we culture MTB in LA-2 medium containing sodium nitrate as source of nitrogen, the SAR of $MTB_{LA\text{-}2}$ cells with magnetosomes arranged in chains can be as high as 4 925.6 W/g (in this work, all SARs are calculated with iron mass) under 764 kHz and 30 kA/m, which is 7.5 times than current commercial magnetic particles within similar size range.

Keyword: magnetotactic bacteria (MTB); hyperthermia; rock magnetism; alternating magnetic field (AMF)

1 INTRODUCTION

Magnetic hyperthermia is an important treatment strategy of diseases based on raising the temperature of local-regional tissues or whole body above physiological value by converting the magnetic energy into thermal energy. It has gone into clinic testing for therapy of malignant tumors due to its intrinsic high tissue penetration and non-invasion (Falk and Issels, 2001; Rosensweig, 2002; Johannsen et al., 2007; Périgo et al., 2015; Blanco-Andujar et al., 2018). Tumor tissues are more susceptible to heat than healthy tissue. When temperatures reach the 41–46 ℃ range (therapeutic window), tumor tissue tends to suffer irreversible damage, while healthy tissue is usually unharmed (Pankhurst et al., 2003; Ortega and Pankhurst, 2013). In clinical trials, it has been proved that hyperthermia combined with conventional treatment modalities (e.g., radiotherapy, chemotherapy) can improve response and survival outcome of tumor patients (Thiesen and Jordan, 2008; Maier-Hauff et al., 2011).

* Supported by the Strategic Priority Research Program of Chinese Academy of Sciences (No. XDB41010403), the National Natural Science Foundation of China (Nos. 41804070, 41774076, 41621004), the Key Program of Chinese Academy of Sciences (No. QYZDJ-SSWDQC024), the Key Research Program of the Institute of Geology and Geophysics, CAS (No. IGGCAS-201903), and the PetroChina Innovation Foundation (No. 2020D-5007-0105)
** Corresponding author: changqiancao@mail.iggcas.ac.cn

During the magnetic hyperthermia treatment process, magnetic nanoparticles (MNPs) with various sizes, ranging from superparamagnetism to magnetic single-domain (roughly 10 up to 100 nm), can be employed to complete the energy conversion through hysteresis loss or Néel/Brownian relaxation process in an alternating magnetic field (AMF) (Rosensweig, 2002; Hergt et al., 2006; Dadfar et al., 2019; Xu and Pan, 2019). Usually, the energy conversion efficiency is expressed by specific absorption rate (SAR), which is defined as the absorbed energy per unit of nanoparticle mass (Mason et al., 2000; Ortega and Pankhurst, 2013). The SAR is directly related to the initial slope of the temperature rising curves, and calculated using the next Eq.1 (Andreu and Natividad, 2013),

$$\mathrm{SAR}=\frac{m_\mathrm{s}}{m_\mathrm{n}}C_\mathrm{p}\frac{\Delta T}{\Delta t}, \tag{1}$$

where m_s is the mass of solvent, m_n is the mass of MNPs, C_p is the heat capacity of solvent, and $\Delta T/\Delta t$ is the initial slope of the temperature rising curve: fitting the curve with Box-Lucas equation [$T(t)=a(1-\mathrm{e}^{-bt})$] to calculate the $\Delta T/\Delta t$ at $t=0$ (Kallumadil et al., 2009). Experimental results show that single-domain particles with narrow size distribution may theoretically provide the most desired heat generation efficiency (Hergt et al., 2008). High SAR ensures enhancement of specific heating power and reduction of dosage applied to the tumor.

MTBs are a kind of aquatic microorganisms that can live in oxic-anoxic interface (OAI) environment and swim along the Earth's magnetic field lines (Blakemore, 1975; Frankel et al., 1997). A unique feature of this type of bacteria is that it has nanometer-sized (30–120 nm) magnetosomes (Fe_3O_4/Fe_3S_4) arranged in chains, which show characteristic single-domain magnetic properties (Bazylinski and Frankel, 2004; Ding et al., 2010; Zhang and Pan, 2018). Magnetosome is a kind of nanomaterial with wide application potential, which has been developed into excellent nanocarriers, such as anti-cancer drug carriers (Sun et al., 2007), transgenic carriers (Yang et al., 2016), and antibody carriers (Li et al., 2010). In addition, MTB Whole cells have been developed into nanobots for antimicrobial benefiting from the unique advantage of self-propulsion capability provided by their flagella and the guidance capabilities ensured by their magnetosome chain (Chen et al., 2019). Magnetosome chains are usually destroyed during extraction; however, the magnetosome crystals coated by membranes still have high heat efficiency due to well-developed crystallinity and particle uniformity (Muela et al., 2016), which are regulated strictly by a series of genes (Uebe and Schüler, 2016). Hergt et al. (2005) reported a maximum SAR value of 960 W/g (calculated with magnetosome mass) for magnetosomes with a mean diameter of 30 nm, under 10 kA/m field amplitude and 410 kHz frequency. Muela et al. (2016) determined a SAR of 2 394 W/g (calculated with magnetosome mass) for magnetosomes of 45 nm exposed to an AMF of 28 kA/m and a frequency of 532 kHz. In addition, each MTB intact cell with magnetosomes arranged in chains can also be used as magnetic hyperthermia agent, and the SAR of the intact cells is usually much higher than that of the isolated magnetosomes because of the low magnetostatic interactions (Fdez-Gubieda et al., 2020). Alphandéry et al. (2011) obtained the SAR value of 860 W/g (calculated with Fe mass) at 88 mT and 108 kHz for MTB intact cells using *Magnetospirillum magneticum* AMB-1 strain. Gandia et al. (2019) directly proved that MTB intact cells had higher SAR than the extracted magnetosomes under the same conditions using *Magnetospirillum gryphiswaldense* MSR-1 strain, and then, the MTB intact cells significantly inhibited the proliferation of cancer cells in AMF. Therefore, MTB whole cells are promising agent for targeted therapy of tumors.

However, the detailed magnetic hyperthermia properties and optimum heat production conditions of MTB cells are not clear. Because the AMF conditions including magnetic field amplitude and frequency providing for testing magnetic hyperthermia treatment are usually limited due to the lack of commercial standard systems. In addition, the SAR value of MTB cells is often measured by home-made equipment under individual conditions. The inconsistency in accuracy and background caloric value produced from magnetic field coil may lead to incomparable results between different laboratories. Hence, benefiting from commercial standard system D5 series (NanoScale Biomagnetics, Zaragoza, Spain) providing AMF with wide range of frequency and amplitude, we implemented a comprehensive study of the hyperthermic response of *Magnetospirillum gryphiswaldense* MSR-1 strain under different magnetic conditions: frequency of 144–764 kHz, and field amplitude of 10–45 kA/m. The heating efficiency was measured using calorimetric method by dual channel fiber optic sensors. We also compared the heating rates of the samples with different magnetic parameters harvested from different medium and

commercial magnetic nanoparticles to determine the hyperthermia mechanisms of MTB cells.

2 MATERIAL AND METHOD

2.1 Preparation of sample

Three samples used in this work, including two MSR-1 samples and a kind of commercial magnetic particle (Fe_3O_4 nanoparticles) with mean size about 30 nm bought from Sangon Biotech (Shanghai), are named MTB_{LA-1}, MTB_{LA-2}, and commercial magnetic particle (S_{cmp}), respectively. MTB_{LA-1} was cultured using medium LA-1 and method reported by Sun et al. (2008). MTB_{LA-2} was harvested from medium LA-2 with sodium nitrate instead of ammonium chloride as sources of nitrogen referred to LA-1 and literature of Heyen and Schüler (2003).

Cell growth and magnetism were assessed by OD_{565} (optical density at 565 nm) and C_{mag} as described by literatures (Schüler et al., 1995). The iron concentrations of the samples were determined by the spectrophotometric ferrozine assay based on the standard curve (0, 0.5, 1, 2, 4, 6, 8, and 10 μg/mL) (Stookey, 1970; Han et al., 2020).

Fresh whole cells were collected by centrifugation at 8 000 r/min for 10 min at 4 ℃ after culturing for 24 h in medium LA-2, and then suspended in water with needed cell concentrations. Samples S_1, S_2, and S_3 were prepared from cells with concentration of OD_{565}=8 through ultrasonic treatment for 0, 10, and 50 min in an ice-water mixture, respectively.

2.2 Transmission electronic microscopy analysis

Morphological characteristics of samples involved in this work were examined by transmission electron microscopy (TEM, JEOL JEM-2100, Tokyo) operating at 200 kV at the Institute of Geology and Geophysics, Chinese Academy of Sciences (Beijing). The sizes of magnetosome were analyzed using standard analytical software. The major and minor axes of magnetosomes were used as the length (L) and width (W) of the crystal, respectively, and the grain size was defined as (L+W)/2.

2.3 Rock magnetic measurements

The measurement of room-temperature hysteresis loops, firstorder reversal curves (FORCs) and saturation isothermal remanent magnetization (SIRM) were performed on a VSM3900 magnetometer (Princeton Measurements Corporation, USA, sensitivity 5.0×10^{-10} Am^2). Hysteresis loops were measured with field increments of 8 mT, ranging between maximum fields of ±1.00 T with an average time of 500 ms. SIRM acquisition curves were obtained with logarithmic increments to a maximum field of 1.00 T. A total of 180 curves for each sample were measured in FORCs using an increasing field step of 1.2 mT with an average time of 400 ms in the range from -50 to 50 mT for B_u and from 0 to 100 mT for B_c. B_u and B_c are two parameters in the FORCs test programs, representing magnetostatic interactions and coercivity of samples. The FORC diagrams were processed using FORCinel version 3.06 software with a smooth factor of 3.

2.4 Magnetic hyperthermia analysis

Magnetic hyperthermia measurements of all samples had been performed using a commercial system D5 series (NanoScale Biomagnetics, Zaragoza, Spain) at the Institute of Geology and Geophysics, Chinese Academy of Sciences (Beijing, China). Samples suspended in water (1.0 mL) in a 2-mL glass chromatography vial were set in the middle of the coil. The temperatures during measurement were recorded by dual channel optic fiber temperature probes with response temperature of 0.1 ℃. One probe was placed in the center of samples, and the other probe was in the gap between glass and coil. Every magnetic field condition was first tested by 1.0-mL water, and the two probes would stabilize to the same temperature, which was the initial temperature of the corresponding testing condition.

The effect of AMF parameters on the heat production efficiency of samples were investigated. Sample MTB_{LA-2} with iron concentration of 48.4 μg/mL was tested at 339 kHz with varying AMF amplitudes (10, 15, 20, 25, 30, 35, 40, and 45 kA/m), and at 30 kA/m with different frequencies (144, 298, 339, 377, 485, 621, and 764 kHz), respectively. All the other tests were performed under the magnetic field condition of 764 kHz and 30 k/Am.

The SAR values were calculated using the Eq.1 as mentioned above, where the solvent was 1-mLwater with the heat capacity of 4.185 J/(g·K).

3 RESULT

3.1 Structural characterizations of MTB cells and magnetosomes

3.1.1 Culture results of MSR-1

After culturing for 24 h, the cells of MTB_{LA-1} and MTB_{LA-2} reached the states of OD_{565}=0.9±0.1,

C_{mag}=0.6±0.1, and OD_{565}=0.9±0.1, C_{mag}=1.8±0.1, respectively. The high OD values imply that both LA-1 with ammonium chloride and LA-2 with sodium nitrate are suitable for the growth of MSR-1 under the culture conditions. Usually, the C_{mag} is well correlated with the average number of magnetosomes per cell and can be used for semi-quantitative assessment of magnetosome formation (Schüler et al., 1995). Thus, the larger C_{mag} value of MTB_{LA-2} indicates that it may contain more magnetosomes, and the medium LA-2 is more suitable for magnetosomes synthesis.

3.1.2 TEM characterization of MTB cells, magnetosomes, and commercial magnetic beads

Figure 1 shows the images of MTB_{LA-1}, MTB_{LA-2} and commercial magnetic particle S_{cmp}. It is obvious that the magnetosomes in MTB_{LA-1} and MTB_{LA-2} are arranged in chains, whereas the S_{cmp} nanoparticles are clustered together (Fig.1a–f). Size analysis reveals that one MTB_{LA-1} cell contains an average of 7.8±3.9 magnetosomes with the average particle size of (27.9±7.9) nm (Fig.1a–b), and the cell of MTB_{LA-2} possess an average of 17.7±5.6 magnetosomes with the average particle size of (35.7±7.7) nm (Fig.1c–d). Compared with MTB_{LA-2}, the MTB_{LA-1} have fewer magnetosomes per cell and bimodal size distributions with a main peak at 32 nm and a secondary peak at 16 nm on the particle size distribution histogram, indicating more immature magnetosomes (Fig.1b), while the MTB_{LA-2} cells have more magnetosomes with larger average particle size, consistent with the results of C_{mag} determination. The true average size of S_{cmp} nanoparticles is (21.2±6.3) nm, which is smaller than the size described in the product specification, possibly due to the statistical errors caused by sample aggregation (Fig.1e–f).

As displayed in Fig.1g, the intact cell structures of the sample S_2 are lost due to ultrasonic treatment for 10 min. With ultrasonic treatment for 50 min, both of the cell structure and magnetosome chain of sample S_3 are completely destroyed, and the magnetosomes stick together (Fig.1h). The sample S_1 is not subjected to any ultrasonic treatment. Therefore, the S_1 remains its original state with complete cell morphology and magnetosome chains.

3.2 Rock magnetic properties

FORC diagrams show very weak magnetostatic interactions ($B_{u,\,1/2}$=1.0 mT) among magnetite particles of MTB cells because of separation by magnetosome membranes and cell structure (Fig.2a–b), which is consistent with our previous reports (Zhang and Pan, 2018). The coercivity value of MTB_{LA-2} ($B_{c,\,FORC}$= 20.4 mT) is larger than that of MTB_{LA-1} ($B_{c,\,FORC}$=17.4 mT), which is in agreement with the TEM results that the MTB_{LA-2} owns larger magnetosomes and longer magnetosome chains (Fig.1a–d). On the contrary, the magnetostatic interactions among magnetite particles in S_{cmp} are significantly stronger ($B_{u,\,1/2}$=9.6 mT) (Fig.2c), and the center of FORC diagram is much closer to the *Y*-axis than that of MTB_{LA-1} and MTB_{LA-2}. This means that the coercivity of S_{cmp} is smaller than MTB cells.

Table 1 Magnetic parameters of different MTBs and S_{cmp}

Sample	MTB_{LA-1}	MTB_{LA-2}	S_{cmp}	S_1	S_2	S_3
B_c (mT)	12.7	18.7	3.8	13.2	7.6	5.5
B_{cr} (mT)	18.0	21.6	9.8	16.8	14.2	13.0
M_s (mAm^2/g)	105.1	116.8	69.5	119.0	112.4	116.6
M_{rs}/M_s	0.37	0.48	0.11	0.44	0.32	0.25

The coercivity (B_c), saturation magnetization (M_s), remanent coercivity (B_{cr}), and saturation remanent magnetization (M_{rs}) of MTB_{LA-1}, MTB_{LA-2}, and S_{cmp} are determined by hysteresis loops and SIRM curves, and the results are shown in Fig.2d and Table 1 (M_s is normalized by iron mass). It is noted that these samples have similar potbelly shape loop, which is characteristic of cubic type of magnetic anisotropy. The MTB_{LA-1}, MTB_{LA-2}, and S_{cmp} samples have B_c values of 12.7, 18.7, and 3.8 mT; M_s values of 105.1, 116.8, and 69.5 mAm^2/g; B_{cr} values of 18.0, 21.6, and 9.8 mT; and M_{rs}/M_s values of 0.37, 0.48, and 0.11, respectively. As a result, the area surrounded by hysteresis loop, in descending order, are MTB_{LA-2}, MTB_{LA-1}, and S_{cmp}, respectively.

The changes in magnetosome chain structure can significantly affect the rock magnetism of MTB cells. The FORCs diagrams of the two ultrasound-treated samples, S_2 and S_3, are clearly different from that of intact cells, S_1, (Fig.2e–g). In particular, there are two hot center spots in FORC diagrams of sample S_3. This might have been caused by chain-structure destruction. As the results of hysteresis loops and SIRMs shown in Table 1; B_c, B_{cr}, and M_{rs}/M_s values of S_1, S_2, and S_3 are reduced in turn, and the corresponding areas of hysteresis loops also decreased in the same order (Fig.2h).

3.3 Heating efficiency of MTB in AMF

As shown in Fig.3a, the temperature rising curves of MTB_{LA-2} under AMF (30 kA/m, 764 kHz) show

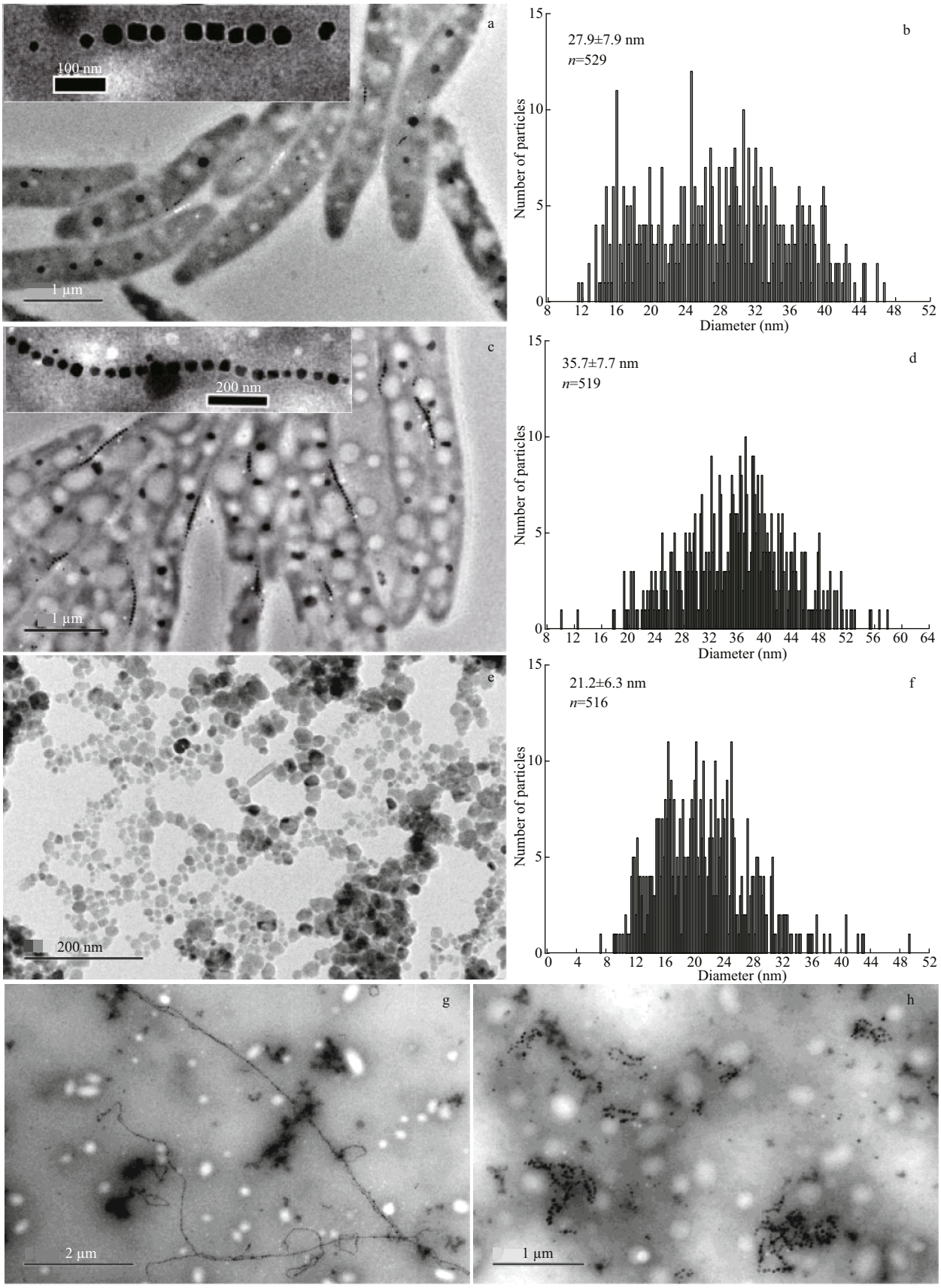

Fig.1 TEM images (a, c, e, g, h) and statistics data of particle size (b, d, f) of MTB samples and commercial magnetic beads

The data inserted in the figure b, d, f represent the average particle size and the number of statistical particles. a–b. MTB_{LA-1}; c–d. MTB_{LA-2}; e–f. S_{cmp}; g. S_2; h. S_3.

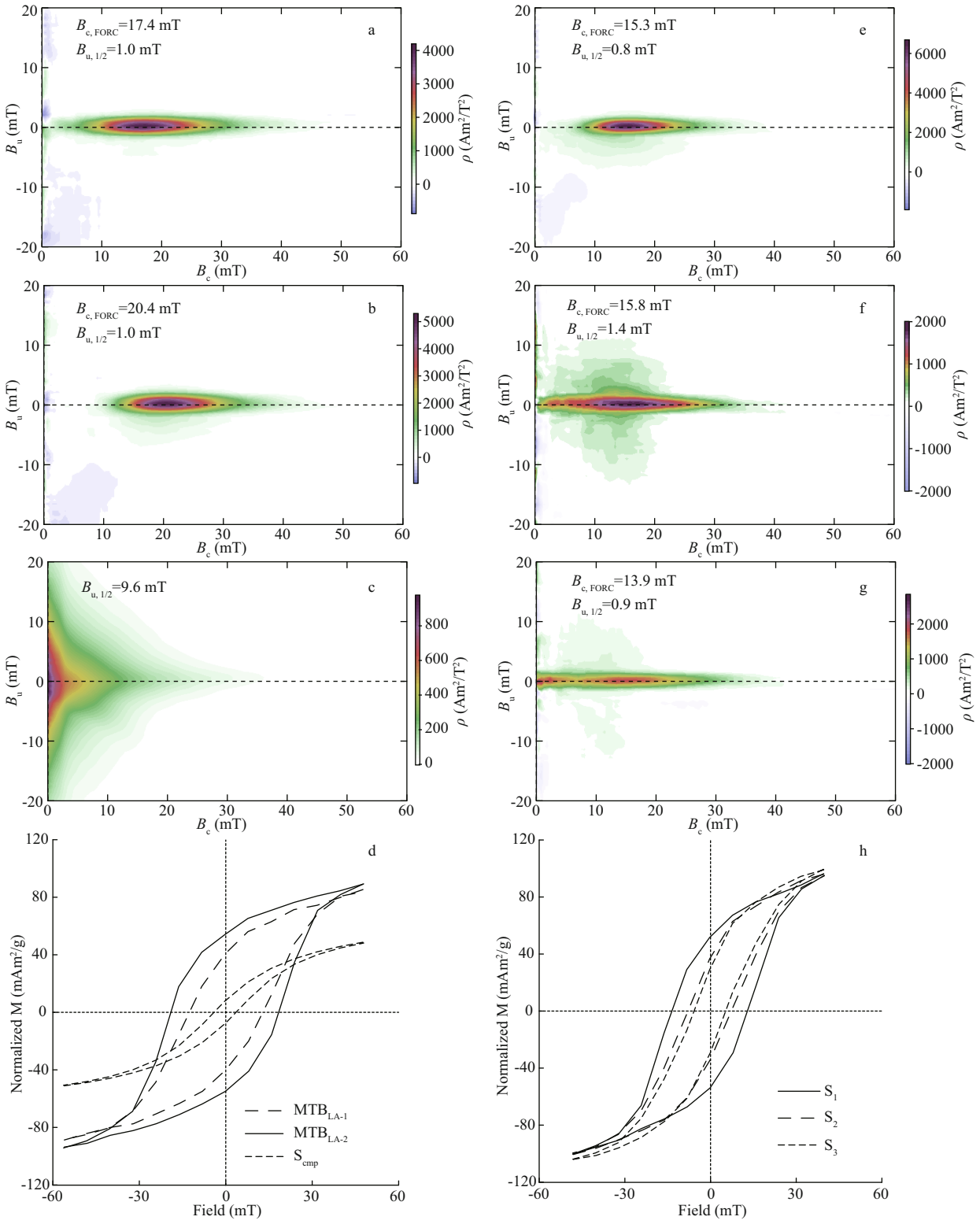

Fig.2 Rock magnetic characterization of samples

a–c. FORC diagrams of MTB_{LA-1}, MTB_{LA-2}, and S_{cmp}; d. room-temperature hysteresis loops of MTB_{LA-1}, MTB_{LA-2}, and S_{cmp}; e–g. FORC diagrams of S_1, S_2, and S_3; h. room-temperature hysteresis loops of S_1, S_2, and S_3. The magnetization was normalized by the mass of Fe.

that the same kind of MTB cells under the same cell concentration (OD=8 or 20) have the same rate of temperature rise in the overlapped curves. This means that the heat production stability of MTB in AMF is stable and repeatable in aqueous medium. The change in temperature (ΔT) values increase linearly with the

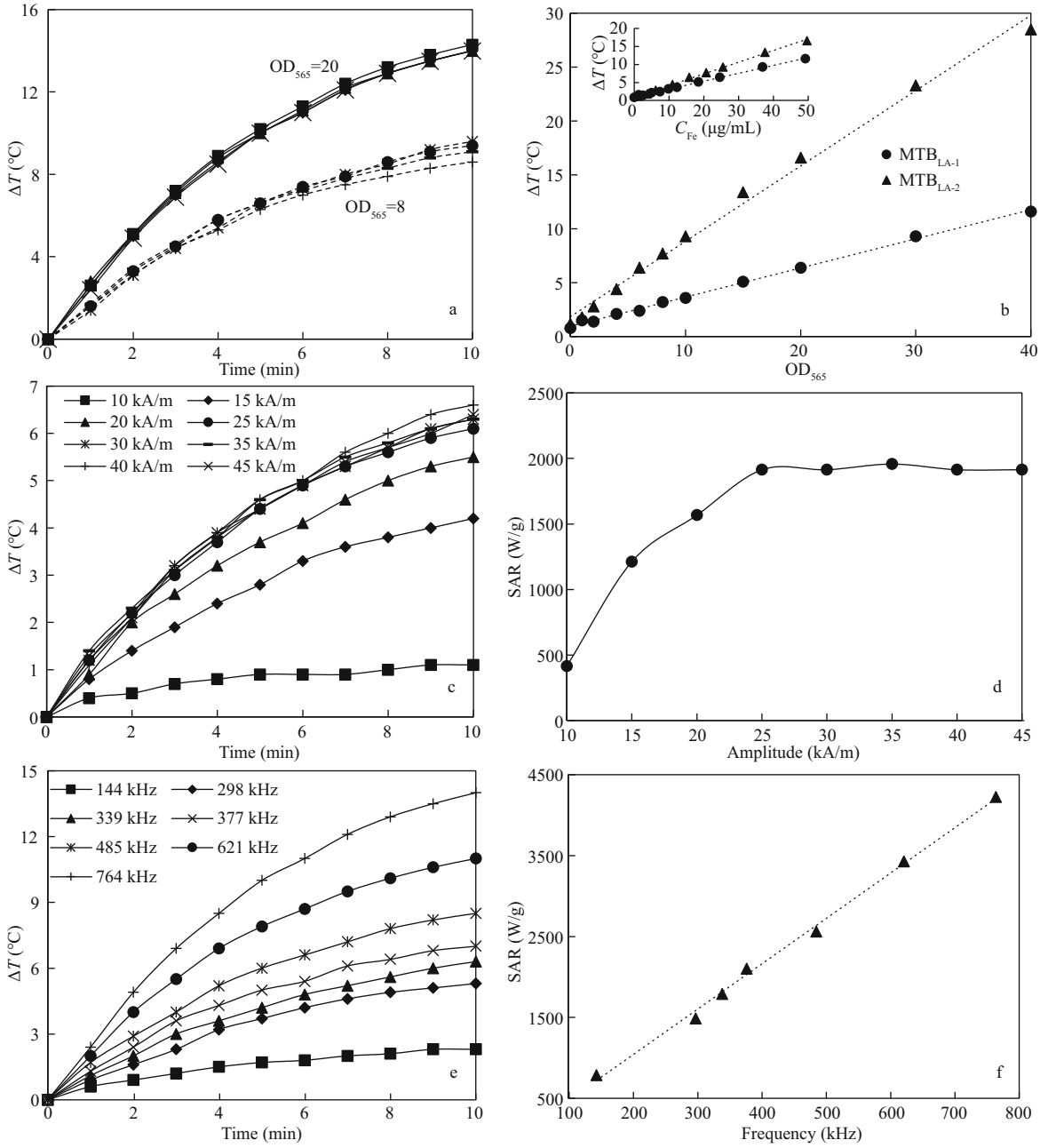

Fig.3 Heating efficiency of MTB cells in AMF

a. repeatability tests of temperature rising curves of MTB in aqueous under AMF with frequency of 764 kHz and amplitude of 30 kA/m, the solid and dashed lines represent MTB_{LA-2} cell concentrations of OD_{565}=20 and OD_{565}=8, respectively; b. ΔT of MTB_{LA-1} and MTB_{LA-2} at 10 min versus cell and iron concentrations; c, d. temperature rising and SAR curves of MTB_{LA-2} with varying amplitude under frequency of 339 kHz; e, f. temperature rising and SAR curves of MTB_{LA-2} with different frequency under amplitude of 30 kA/m.

concentration of MTB cells (Fig.3b). At the same iron concentration, the ΔT of MTB_{LA-2} at 10 min is higher than that of MTB_{LA-1} (Fig.3b insert), indicating that the magnetosomes of MTB_{LA-2} have stronger heat conversion ability. This is consistent with the results of TEM (Fig.1a–d) and magnetic characterization (Fig.2a–b); therefore, the MTB_{LA-2} cells with more and larger magnetosomes have superior magnetic properties and heat conversion efficiency.

In order to evaluate the effect of magnetic field amplitude on the heat production efficiency of MTB, we tested the temperature rising curves of MTB_{LA-2} with iron concentration of 48.4 μg/mL using AMF frequency of 339 kHz at different amplitudes of 10, 15, 20, 25, 30, 35, 40, 45 kA/m. As AMF amplitude increased from 10 to 25 kA/m, the ΔT rises from 1.1 to 6.1 ℃ in 10 min, and the SARs of MTB_{LA-2} are increased from 415.7 to 1 913.8 W/g (Fig.3c–d).

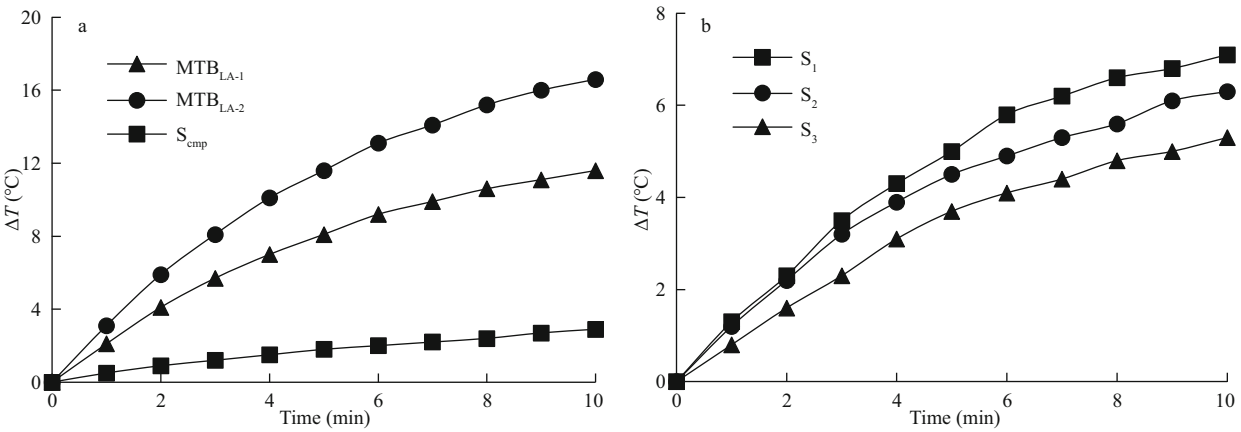

Fig.4 Temperature rising curves under amplitude of 30 kA/m and frequency of 764 kHz

a. MTB$_{LA-1}$, MTB$_{LA-2}$, and S$_{cmp}$; b. S$_1$, S$_2$, and S$_3$.

However, the ΔT and SARs stop increasing with the amplitude when the amplitude exceeded 25 kA/m.

To understand the effect of frequency on heat efficiency of MTB cells, we also perform heating test using the sample MTB$_{LA-2}$ with iron concentration of 48.4 μg/mL as AMF frequency increased from 144 to 764 kHz under the constant amplitude of 30 kA/m. With the frequency increased, the ΔT grows from 2.4 to 14.0 ℃ at 10 min (Fig.3e), and SARs grow linearly from 788.0 to 4 226.0 W/g (Fig.3f).

3.4 Comparison of heat production efficiency between MTB and S$_{cmp}$

The temperature rising curves of MTB$_{LA-1}$, MTB$_{LA-2}$, and S$_{cmp}$ with same iron concentration of 49.2 μg/mL are tested under amplitude of 30 kA/m and frequency of 764 kHz. The ΔT values at 10 min are 11.6 ℃ for MTB$_{LA-1}$, 16.6 ℃ for MTB$_{LA-2}$, and 2.9 ℃ for S$_{cmp}$, respectively (Fig.4a), and the corresponding SAR values are 3 440.2 W/g for MTB$_{LA-1}$, 4 925.6 W/g for MTB$_{LA-2}$, and 657.3 W/g for S$_{cmp}$, respectively. As expected, sample MTB$_{LA-2}$ with more and larger magnetosomes possesses stronger ability of heat generation than sample MTB$_{LA-1}$. Both of the two MTB samples produce more heat than commercial magnetic beads under the same conditions because of the advantages in magnetic properties, such as B_c, M_s, M_{rs}/M_s.

3.5 Effect of magnetosome chains on heat production of MTB

To evaluate the effect of magnetosome chain integrity on heat production, the temperature rising curves of sample S$_1$, S$_2$, and S$_3$ with same iron concentration of 22.3 μg/mL are tested under amplitude of 30 kA/m and frequency of 764 kHz, and the corresponding SAR values were calculated according to the temperature rising curves. It is obvious that the sample S$_1$ owing to intact cell structure and magnetosome chain exhibit the strongest ability of heat production with ΔT value of 7.1 ℃ at 10 min (Fig.4b). By contrast, the ΔT values of S$_2$ and S$_3$ at 10 min are only 6.3 ℃ and 5.3 ℃, respectively. Likewise, the SAR of S$_1$ is 4 643.6 W/g, which is larger than that of S$_2$ (4 209.4 W/g) and S$_3$ (3 114.6 W/g). This highlights the important role of the intact magnetosome chain for heat generation during the magnetic hyperthermia process.

4 DISCUSSION

There are three physical principles involved in the heat transfer mechanisms involved in magnetic hyperthermia, namely: (i) resistance heating due to eddy currents, (ii) magnetic heating due to hysteresis loss, and (iii) magnetic heating due to Néel and Brownian relaxation processes (Ortega and Pankhurst, 2013). In the case of single-domain particles, hysteresis losses are higher than any of the other losses (Hergt et al., 1998). When the magnetic field vary with time, the relationship between the area under AC hysteresis loop and the amount of heat generated per cycle (P_{FM}) follows the next equation:

$$P_{FM} = \mu_0 f \oint H \mathrm{d}M, \quad (2)$$

where f is the frequency of the applied field, H is the field amplitude and M is the magnetization. It is well known that magnetosomes belong to single-domain magnetic particles (Ding et al., 2010; Zhang and Pan, 2018), and MTB shows typical rock magnetic characteristics of single-domain (Fig.2a–d), thus the magnetic hyperthermia mechanism of MTB mainly follows the principle of hysteresis loss. The experimental results accord with the prediction of the

Eq.2: (i) ΔT and SARs linearly increase with field frequency; (ii) ΔT and SARs increase with field amplitude only within a certain range. When the magnetization of MTB is saturated and the area under the AC hysteresis loop reaches maximum, ΔT and SARs will no longer increase with the amplitude. In a word, the three main parameters of AC hysteresis loop, M_s, M_{rs}, and B_c, determine the area under AC hysteresis loop, and thus determine the heat production efficiency of single domain particles at the same frequency. Unfortunately, due to the limitation of equipment, we only test the low-frequency hysteresis loop, which could not be directly used in the calculation of heat production efficiency, but could be used to evaluate the capacity of heat generation of the samples.

It is obvious that the MTB whole cells have huge advantages in heat production compared with commercial magnetic particles under the conditions of nearly similar particle size, same iron concentration and magnetic field. Under the experimental conditions described above, the ΔT values of MTB_{LA-1} and MTB_{LA-2} at 10 min are 3 times and 4.7 times more than that of sample S_{cmp}, respectively (Fig.4a). As the values of B_c, M_s, and M_{rs}/M_s of MTB are significantly greater than those of sample S_{cmp}, it means the lager value of AC hysteresis loop area and higher capacity of heat generation. Comparing with the sample S_{cmp}, the magnetic parameters and heat production efficiency of MTB whole cells greatly benefit from the inherent chain-like arrangement of magnetosomes.

Combined the rock magnetic and hyperthermia measurements, it indicates that the chain alignment of magnetosomes plays important roles in the magnetic parameters and heating efficiency of MTB intact cells. The destruction of the magnetosome chain is directly proportional to the decrease in magnetic parameters, such as B_c, B_{cr}, and M_{rs}/M_s (Li et al., 2012). Magnetic hyperthermia also follows the same law (Fig.4b). The MTB intact cell organizes magnetosomes like necklaces through magnetosome membrane and cytoskeletal proteins, which reduces the interaction between magnetic particles and increases magnetic anisotropy and coercivity. The excellent magnetic properties make MTB whole cells have great heat production efficiency and promising medical application prospects.

The MTB whole cells used in this study shows excellent property in heat production; however, there are still some limitations. For safety and patient tolerance reasons, the applied magnetic field is limited in clinical magnetic hyperthermia therapy by "Brezovich criterion" (Brezovich, 1988). In this case, achieving the "therapeutic window" of tumor would requires 10^9 magnitude of bacteria, equivalent to a dose of approximately 1-mL OD_{565}=20 bacteria cells with iron concentration of about 49.2 μg/mL, because one single MSR-1 cell contains only limited number of magnetosomes, averaging of 17.7 per cell in our study. Large number of foreign bacteria entering the body is bound to increase the safety risk. One strategy for reducing the dose of MTB is to continue to improve the heat production efficiency of unit MTB cells. Our study and previous literatures show that using sodium nitrate instead of ammonium chloride as medium nitrogen source could significantly improve the parameters of magnetosome (Heyen and Schüler, 2003), and then improve the heat production efficiency. Li et al. (2016) proves that cobalt-containing magnetosomes with higher coercivity could be synthesized by adding cobalt to the culture medium. It is well known that MSR-1 cultured in fermenter have higher C_{mag} value than that cultured in shaking table (Zhang et al., 2011), indicating higher coercivity and greater efficiency in heat generation. All these indicate that the MSR-1 cells with higher heat efficiency can be obtained by optimizing medium and culture mode. In addition, as more and more species of MTB have been discovered, we are pleasantly surprised to find a kind of giant rod-shaped MTB containing hundreds of magnetosomes per cell (Lin et al., 2009; Li et al., 2020), which means huge heat efficiency and potential for clinical application. However, the vast majority of MTB, including giant rod-shaped MTB, have not achieved pure culture at present. Therefore, it is very significant to study the culture of MTB in future.

5 CONCLUSION

MTB whole cells with single-domain magnetosome exhibit excellent magnetic hyperthermia ability, and the heat generation principle mainly follows the hysteresis loss mechanism. So the heat production efficiency of MTB cells is closely related to the parameters of hysteresis loop, such as B_c, M_s, and M_{rs}. Benefitting from the chain structures of magnetosomes, MTB cells have more superior magnetic properties than commercial magnetic beads with similar size, and thus have higher efficiency in heat production. As expected, MTB cells with more and larger magnetosomes possess greater efficiency in heat production. Therefore, improving the magnetic

properties of MTB cells by optimizing the medium and culture method may further improve the heat conversion efficiency.

6 DATA AVAILABILITY STATEMENT

The data that support the findings of the current study are available on reasonable request from the corresponding author.

7 ACKNOWLEDGMENT

We thank Tang XU from the Institute of Geology and Geophysics, CAS for his help in TEM analysis.

References

Alphandéry E, Faure S, Raison L, Duguet E, Howse P A, Bazylinski D A. 2011. Heat production by bacterial magnetosomes exposed to an oscillating magnetic field. *The Journal of Physical Chemistry C*, **115**(1): 18-22, https://doi.org/10.1021/jp104580t.

Andreu I, Natividad E. 2013. Accuracy of available methods for quantifying the heat power generation of nanoparticles for magnetic hyperthermia. *International Journal of Hyperthermia*, **29**(8): 739-751, https://doi.org/10.3109/02656736.2013.826825.

Bazylinski D A, Frankel R B. 2004. Magnetosome formation in prokaryotes. *Nature Reviews Microbiology*, **2**(3): 217-230, https://doi.org/10.1038/nrmicro842.

Blakemore R. 1975. Magnetotactic bacteria. *Science*, **190**(4212): 377-379, https://doi.org/10.1126/science. 170679.

Blanco-Andujar C, Teran F J, Ortega D. 2018. Chapter 8: Current Outlook and Perspectives on Nanoparticle-Mediated Magnetic Hyperthermia. Iron Oxide Nanoparticles for Biomedical Applications: Synthesis, Functionalization and Application. Elsevier. p.197-245.

Brezovich I A. 1988. Low frequency hyperthermia: capacitive and ferromagnetic thermoseed methods. *Medical Physics Monograph*, **16**: 82-111.

Chen C Y, Chen L J, Wang P P, Wu L F, Song T. 2019. Steering of magnetotactic bacterial microrobots by focusing magnetic field for targeted pathogen killing. *Journal of Magnetism and Magnetic Materials*, **479**: 74-83, https://doi.org/10.1016/j.jmmm.2019.02.004.

Dadfar S M, Roemhild K, Drude N I, Von Stillfried S, Knüchel R, Kiessling F, Lammers T. 2019. Iron oxide nanoparticles: diagnostic, therapeutic and theranostic applications. *Advanced Drug Delivery Reviews*, **138**: 302-325, https://doi.org/10.1016/j.addr.2019.01.005.

Ding Y, Li J H, Liu J N, Yang J, Jiang W, Tian J S, Li T, Pan Y X, Li J L. 2010. Deletion of the *ftsZ*-like gene results in the production of superparamagnetic magnetite magnetosomes in *Magnetospirillum gryphiswaldense*. *Journal of Bacteriology*, **192**(4): 1097-1105, https://doi.org/10.1128/JB.01292-09.

Falk M H, Issels R D. 2001. Hyperthermia in oncology. *International Journal of Hyperthermia*, **17**(1): 1-18, https://doi.org/10.1080/02656730150201552.

Fdez-Gubieda M L, Alonso J, García-Prieto A, García-Arribas A, Barquín L F, Muela A. 2020. Magnetotactic bacteria for cancer therapy. *Journal of Applied Physics*, **128**(7): 070902, https://doi.org/10.1063/5.0018036.

Frankel R B, Bazylinski D A, Johnson M S, Taylor B L. 1997. Magneto-aerotaxis in marine coccoid bacteria. *Biophysical Journal*, **73**(2): 994-1000, https://doi.org/10.1016/S0006-3495(97)78132-3.

Gandia D, Gandarias L, Rodrigo I, Robles-García J, Das R, Garaio E, García J Á, Phan M H, Srikanth H, Orue I, Alonso J, Muela A, Gubieda M L F. 2019. Unlocking the potential of magnetotactic bacteria as magnetic hyperthermia agents. *Small*, **15**(41): 1902626, https://doi.org/10.1002/smll.201902626.

Han X H, Tomaszewski E J, Sorwat J, Pan Y X, Kappler A, Byrne J M. 2020. Effect of microbial biomass and humic acids on abiotic and biotic magnetite formation. *Environmental Science & Technology*, **54**(7): 4121-4130, https://doi.org/10.1021/acs.est.9b07095.

Hergt R, Andra W, d'Ambly C G, Hilger I, Kaiser W A, Richter U, Schmidt H G. 1998. Physical limits of hyperthermia using magnetite fine particles. *IEEE Transactions on Magnetics*, **34**(5): 3745-3754, https://doi.org/10.1109/20.718537.

Hergt R, Dutz S, Müller R, Zeisberger M. 2006. Magnetic particle hyperthermia: nanoparticle magnetism and materials development for cancer therapy. *Journal of Physics*: *Condensed Matter*, **18**(38): S2919, https://doi.org/10.1088/0953-8984/18/38/S26.

Hergt R, Dutz S, Röder M. 2008. Effects of size distribution on hysteresis losses of magnetic nanoparticles for hyperthermia. *Journal of Physics*: *Condensed Matter*, **20**(38): 385214, https://doi.org/10.1088/0953-8984/20/38/385214.

Hergt R, Hiergeist R, Zeisberger M, Schüler D, Heyen U, Hilger I, Kaiser W A. 2005. Magnetic properties of bacterial magnetosomes as potential diagnostic and therapeutic tools. *Journal of Magnetism and Magnetic Materials*, **293**(1): 80-86, https://doi.org/10.1016/j.jmmm.2005.01.047.

Heyen U, Schüler D. 2003. Growth and magnetosome formation by microaerophilic *Magnetospirillum* strains in an oxygen-controlled fermentor. *Applied Microbiology and Biotechnology*, **61**(5): 536-544, https://doi.org/10.1007/s00253-002-1219-x.

Johannsen M, Gneveckow U, Thiesen B, Taymoorian K, Cho C H, Waldöfner N, Scholz R, Jordan A, Loening S A, Wust P. 2007. Thermotherapy of prostate cancer using magnetic nanoparticles: feasibility, imaging, and three-dimensional temperature distribution. *European Urology*, **52**(6): 1653-1662, https://doi.org/10.1016/j.eururo.2006.11.023.

Kallumadil M, Tada M, Nakagawa T, Abe M, Southern P, Pankhurst Q A. 2009. Suitability of commercial colloids for magnetic hyperthermia. *Journal of Magnetism and*

Magnetic Materials, **321**(10): 1509-1513, https://doi.org/10.1016/j.jmmm.2009.02.075.

Li A H, Tang T, Zhang H Y, Wang Q, Tian J S, Li Y. 2010. Modification of Bacterial magnetosomes and application of magnetosome-antibody complex in pathogen detection. *Acta Biophysica Sinica*, **26**(8): 680-690. (in Chinese with English abstract)

Li J H, Liu P Y, Wang J, Roberts A P, Pan Y X. 2020. Magnetotaxis as an adaptation to enable bacterial shuttling of microbial sulfur and sulfur cycling across aquatic oxic-anoxic interfaces. *Journal of Geophysical Research*: *Biogeosciences*, **125**(12): e2020JG006012, https://doi.org/10.1029/2020JG006012.

Li J H, Menguy N, Arrio M A, Sainctavit P, Juhin A, Wang Y Z, Chen H T, Bunau O, Otero E, Ohresser P, Pan Y X. 2016. Controlled cobalt doping in the spinel structure of magnetosome magnetite: new evidences from element- and site-specific X-ray magnetic circular dichroism analyses. *Journal of the Royal Society Interface*, **13**(121): 20160355, https://doi.org/10.1098/rsif.2016.0355.

Li J H, Wu W F, Liu Q S, Pan Y X. 2012. Magnetic anisotropy, magnetostatic interactions and identification of magnetofossils. *Geochemistry*, *Geophysics*, *Geosystems*, **13**(12): Q10Z51, https://doi.org/10.1029/2012GC004384.

Lin W, Li J H, Schüler D, Jogler C, Pan Y X. 2009. Diversity analysis of magnetotactic bacteria in Lake Miyun, northern China, by restriction fragment length polymorphism. *Systematic and Applied Microbiology*, **32**(5): 342-350, https://doi.org/10.1016/j.syapm.2008.10.005.

Maier-Hauff K, Ulrich F, Nestler D, Niehoff H, Wust P, Thiesen B, Orawa H, Budach V, Jordan A. 2011. Efficacy and safety of intratumoral thermotherapy using magnetic iron-oxide nanoparticles combined with external beam radiotherapy on patients with recurrent glioblastoma multiforme. *Journal of Neuro-Oncology*, **103**(2): 317-324, https://doi.org/10.1007/s11060-010-0389-0.

Mason P A, Hurt W D, Walters T J, D'Andrea J A, Ryan K L, Nelson D A, Smith K I, Ziriax J M. 2000. Effects of frequency, permittivity, and voxel size on predicted specific absorption rate values in biological tissue during electromagnetic-field exposure. *IEEE Transactions on Microwave Theory and Techniques*, **48**(11): 2050-2058, https://doi.org/10.1109/22.884194.

Muela A, Muñoz D, Martin-Rodriguez R, Orue I, Garaio E, de Cerio A A D, Alonso J, García J Á, Fdez-Gubieda M L. 2016. Optimal parameters for hyperthermia treatment using biomineralized magnetite nanoparticles: theoretical and experimental approach. *The Journal of Physical Chemistry C*, **120**(42): 24437-24448, https://doi.org/10.1021/acs.jpcc.6b07321.

Ortega D, Pankhurst Q A. 2013. Magnetic hyperthermia. *In*: P. O'Brien. Nanoscience: Volume 1: Nanostructures through Chemistry. Royal Society of Chemistry: Cambridge. p.60-88, https://doi.org/10.1039/9781849734844-00060.

Pankhurst Q A, Connolly J, Jones S K, Dobson J. 2003. Applications of magnetic nanoparticles in biomedicine. *Journal of Physics D*: *Applied Physics*, **36**(13): R167, https://doi.org/10.1088/0022-3727/36/13/201.

Périgo E A, Hemery G, Sandre O, Ortega D, Garaio E, Plazaola F, Teran F J. 2015. Fundamentals and advances in magnetic hyperthermia. *Applied Physics Reviews*, **2**(4): 041302, https://doi.org/10.1063/1.4935688.

Rosensweig R E. 2002. Heating magnetic fluid with alternating magnetic field. *Journal of Magnetism and Magnetic Materials*, **252**: 370-374, https://doi.org/10.1016/S0304-8853(02)00706-0.

Schüler D, Uhl R, Bäuerlein E. 1995. A simple light scattering method to assay magnetism in Magnetospirillum gryphiswaldense. *FEMS Microbiology Letters*, **132**(1-2): 139-145, https://doi.org/10.1111/j.1574-6968.1995.tb07823.x.

Stookey L L. 1970. Ferrozine—a new spectrophotometric reagent for iron. *Analytical Chemistry*, **42**(7): 779-781, https://doi.org/10.1021/ac60289a016.

Sun J B, Duan J H, Dai S L, Ren J, Zhang Y D, Tian J S, Li Y. 2007. *In vitro* and *in vivo* antitumor effects of doxorubicin loaded with bacterial magnetosomes (DBMs) on H22 cells: the magnetic bio-nanoparticles as drug carriers. *Cancer Letters*, **258**(1): 109-117, https://doi.org/10.1016/j.canlet.2007.08.018.

Sun J B, Zhao F, Tang T, Jiang W, Tian J S, Li Y, Li J L. 2008. High-yield growth and magnetosome formation by *Magnetospirillum gryphiswaldense* MSR-1 in an oxygen-controlled fermentor supplied solely with air. *Applied Microbiology and Biotechnology*, **79**(3): 389-397, https://doi.org/10.1007/s00253-008-1453-y.

Thiesen B, Jordan A. 2008. Clinical applications of magnetic nanoparticles for hyperthermia. *International Journal of Hyperthermia*, **24**(6): 467-474, https://doi.org/10.1080/02656730802104757.

Uebe R, Schüler D. 2016. Magnetosome biogenesis in magnetotactic bacteria. *Nature Reviews Microbiology*, **14**(10): 621-637, https://doi.org/10.1038/nrmicro.2016.99.

Xu H T, Pan Y X. 2019. Experimental evaluation on the heating efficiency of magnetoferritin nanoparticles in an alternating magnetic field. *Nanomaterials*, **9**(10): 1457, https://doi.org/10.3390/nano9101457.

Yang W J, Bai Y, Wang X, Dong X X, Li Y, Fang M Y. 2016. Attaching biosynthesized bacterial magnetic particles to polyethylenimine enhances gene delivery into mammalian cells. *Journal of Biomedical Nanotechnology*, **12**(4): 789-799, https://doi.org/10.1166/jbn.2016.2213.

Zhang T W, Pan Y X. 2018. Constraining the magnetic properties of ultrafine-and fine-grained biogenic magnetite. *Earth*, *Planets and Space*, **70**(1): 206, https://doi.org/10.1186/s40623-018-0978-2.

Zhang Y, Zhang X J, Jiang W, Li Y, Li J L. 2011. Semicontinuous culture of *Magnetospirillum gryphiswaldense* MSR-1 cells in an autofermentor by nutrient-balanced and isosmotic feeding strategies. *Applied and Environmental Microbiology*, **77**(17): 5851-5856, https://doi.org/10.1128/AEM.05962-11.